Hindawi
International Journal of Aerospace Engineering
Volume 2019, Article ID 5847627, 15 pages
https://doi.org/10.1155/2019/5847627

Research Article

Static Aeroelastic Characteristics of Morphing Trailing-Edge Wing Using Geometrically Exact Vortex Lattice Method

Sen Mao, Changchuan Xie, Lan Yang, and Chao Yang

School of Aeronautic Science and Engineering, Beihang University, 100191 Beijing, China

Correspondence should be addressed to Changchuan Xie; xiechangc@buaa.edu.cn

Received 19 May 2019; Accepted 30 August 2019; Published 16 November 2019

Academic Editor: Rosario Pecora

A morphing trailing-edge (TE) wing is an important morphing mode in aircraft design. In order to explore the static aeroelastic characteristics of a morphing TE wing, an efficient and feasible method for static aeroelastic analysis has been developed in this paper. A geometrically exact vortex lattice method (VLM) is applied to calculate the aerodynamic forces. Firstly, a typical model of a morphing TE wing is chosen and built which has an active morphing trailing edge driven by a piezoelectric patch. Then, the paper carries out the static aeroelastic analysis of the morphing TE wing and corresponding simulations were carried out. Finally, the analysis results are compared with those of a traditional wing with a rigid trailing edge using the traditional linearized VLM. The results indicate that the geometrically exact VLM can better describe the aerodynamic nonlinearity of a morphing TE wing in consideration of geometrical deformation in aeroelastic analysis. Moreover, out of consideration of the angle of attack, the deflection angle of the trailing edge, among others, the wing system does not show divergence but bifurcation. Consequently, the aeroelastic analysis method proposed in this paper is more applicable to the analysis and design of a morphing TE wing.

1. Introduction

Morphing aircraft can change the shape of air vehicles and vehicle components to adapt to a changing mission environment and achieve the best flight performance in a variety of missions. Compared with other morphing aircraft designs, a morphing TE wing outstandingly improves the aerodynamic characteristics of the aircraft. It also has a remarkable influence on low-speed cruise and on the take-off and landing of aircrafts. There are many structural forms of morphing TE wings such as a traditional morphing TE wing which is a hinged structure driven by a motor and a smart structure TE morphing wing based on smart materials [1]. Each morphing TE wing has its own advantages and disadvantages.

A growing body of research is dedicated to the application of piezoelectric materials to a morphing wing. FlexSys Inc. of USA designed a wing structure that can achieve continuous variable camber, with a trailing-edge deflection of -10°~+10°. The wing based on a piezoelectric ceramic driver serves to achieve high frequency wing rapid deformation [2]. Kansas University has conducted research on a novel piezoelectric actuator to drive tip deformation of microaircraft [3]. Flight tests showed excellent roll control of the piezoelectric actuator for the microaircraft. In the same year, the Canadian National Research Council Institute of Aeronautics developed a flexible curved wing with MFCs [4]. The MFCs were employed to drive the trailing edge of the wing to bend. Moreover, Onur Bilgen from Virginia Tech University (USA) designed a control system for wingtip torsional deformation of microaircraft by virtue of a macrofiber composite (MFC) and tested the driving performance of MFC for glass fiber composite patches [5]. Wind tunnel tests were conducted to study the difference between the trailing-edge control and the MFC driving wing. The results demonstrated that the resistance of the MFC-driven composite wing is lower, and the driving bandwidth is wider. The flight test was successfully carried out then. Afterward, the German Aerospace Center conducted an active torsional rotor research [6] by embedding piezofiber composite actuators with different lay angles in the rotor. Furthermore, a span-wise morphing trailing-edge concept was proposed by Pankonien and Inman in a modular design of 12 alternating active and

passive aileron sections [7]. The active ailerons were driven by macrofiber composites which bent the trailing edge to cause a smooth chord-wise camber change of airfoils. Also, wind tunnel tests at a flow speed of 10 m/s were carried out by virtue of a hardware demonstrator. Results indicated that the developed span-wise morphing trailing edge led to excellent aerodynamic and structural performance. In addition, Ohanian et al. and Kochersberger et al. compared a novel morphing control surface design employing piezoelectric MFC actuators with a servo-actuated system [8–10]. A comprehensive comparison including aerodynamics, size, weight, power, bandwidth, and reliability has been extended to include flight test comparisons. The morphing actuation scheme demonstrated a control bandwidth that was an order of magnitude greater than for the servo-actuated system, but showed a 12% decrease in roll rate when compared to the servo-actuated baseline aircraft. Flight tests are planned to fully prove the benefits of the morphing actuation which achieved 1 million cycles without failure and minimal degradation over a servo-actuated design.

However, there are still deficiencies in these studies. Firstly, the aerodynamic forces in the previous studies are all calculated based on CFD, which can inarguably generate accurate aerodynamic results but not lend itself to structure optimization and control system design of the morphing wing due to its time-consuming nature. Secondly, most previous researches concentrated on the realization of a deformation mechanism without giving equal prominence to the effects of wing deformation on the aerodynamics. At last, in these studies, the aeroelastic characteristics were examined only after the design had been completed, which renders it difficult to remedy potential design flaws. Different from the above research, Li et al. made an investigation into the nonlinear aeroelastic behavior of a composite wing with morphing trailing edge actuated by curved beams [11]. In the analysis, a doublet lattice method was used to calculate unsteady aerodynamic force. Results suggested that wing deformation was correlated with aeroelastic responses of the composite wing. In addition, the aeroelastic method based on VLM is very mature. Stanford and Beran optimized the design of a flapping wing in forward flight with active shape morphing using an inviscid three-dimensional unsteady vortex-lattice method [12]. Xie et al. used a nonplanar VLM to compute the nonplanar aerodynamics of flexible wings with large deformation [13]. The VLM boasts a moderate level of fidelity and a relatively inexpensive cost of computation. However, as a result of the linearization of boundary conditions, the traditional linear VLM loses sight of the influence of geometric deformation on an aerodynamic influence coefficient matrix. This method is not applicable to the aeroelastic analysis of a morphing wing, especially when the aerodynamic shape is changed significantly compared with the initial one. To offset the aforementioned deficiencies, a new aerodynamic calculation method based on nonplanar VLM is proposed herein to serve as a static aeroelastic analysis method for a morphing TE wing. This new method can play a better role in shedding light on the aerodynamic characteristics of the 2D wing with the control surface than the conventional linearized VLM, hereinafter referred to as geometrically exact VLM.

In Section 2, a 2D wing with an active morphing trailing edge driven by a piezoelectric patch was chosen as the research object to analyze its static aeroelastic characteristics. In Section 3, a set of numerical validations are carried out and the analysis results are compared with traditional wings with a rigid trailing edge by the traditional linearized VLM. The results not only theoretically deepen the understanding of the aerodynamic and aeroelastic characteristics of a morphing TE wing, but they also provide the theoretical basis for further research on a comprehensively optimized design of a morphing TE wing.

2. Methodology

2.1. Morphing Piezoelectric Wing Model. The main purpose of this paper is to establish a clear and accurate aeroelastic formulation of the morphing TE wing and shed light on its aeroelastic properties by virtue of the geometrically exact VLM. Thus, a typical and simple model of the morphing TE wing is chosen and analyzed which has an active morphing trailing edge driven by a piezoelectric patch, hereinafter referred to as the morphing piezoelectric wing. In particular, there is no gap between the wing and the active morphing trailing edge, as opposed to traditional wings with a rigid trailing edge. The morphing piezoelectric wing is modeled as a beam, as shown in Figure 1. X-0-Y is a rectangular coordinate system on the ground. x-0-y is the rectangular coordinate system for the rigid part of the wing, while s-0-n is the rectangular coordinate system for the elastic bending part of the wing. The piezoelectric patch covers the trailing edge of the wing which is taken as the active morphing trailing edge, and the length of the trailing edge is denoted as l_2, while the length of the other part of the wing is denoted as l_1. According to the characteristics of the piezoelectric patches, the bending moment M_P is generated to deform the beam when a voltage is added to both ends of the patch. The voltage is denoted as piezoelectric voltage U, and the trailing-edge deflection angle is denoted as β. A torsion spring is installed, of which the stiffness is equivalent to the pitch stiffness K_θ. The angle of attack is α, and the pitch angle is θ. It is generally considered that the wing profile is rigid. And all deformation of the beam is assumed to be caused by piezoelectric torque. The entire wing rotates around the torsion spring under aerodynamic load. This is therefore a simple rigid-elastic coupling dynamics model. Meanwhile, the simulation does not take into account the piezoelectric voltage limit, the installation form of the piezoelectric patches, and the nonlinear factors of the piezoelectric patches.

2.2. Piezoelectric Trailing Edge Deformation. The geometrical deformation of the trailing-edge may be considerable under the action of piezoelectric moments in Figure 1. Therefore, a small deformation assumption is not used when describing wing deformation in this paper. This is a geometric nonlinear problem with large deformation and small strain. The

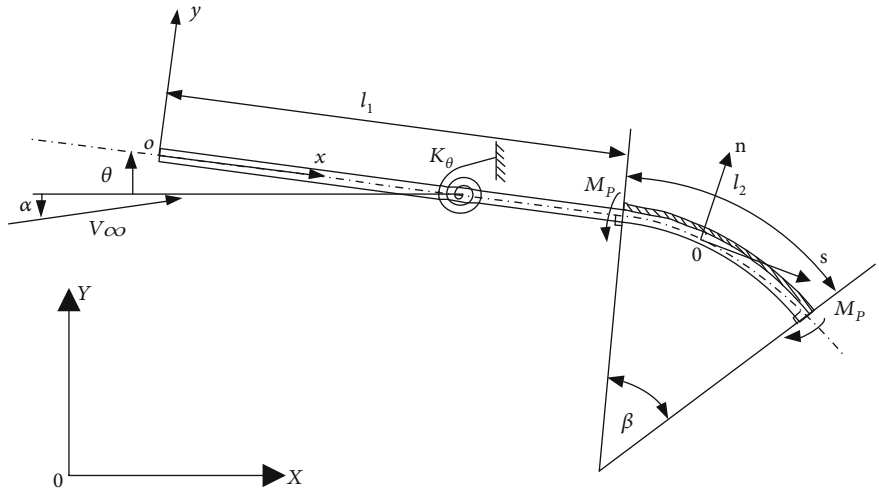

Figure 1: The morphing piezoelectric wing model.

bending strain ε in the cross section can be obtained through the linear constitutive equation:

$$\varepsilon = \frac{n}{\rho}, \tag{1}$$

where ρ represents the radius of curvature of the trailing-edge and n represents the distance from the neutral layer.

The upper surface bending strain ε_s is as follows:

$$\varepsilon_s = \frac{H}{2\rho}, \tag{2}$$

where H represents the thickness of the trailing-edge.

The relationship between the bending moment of the beam M_s and the deformation of the beam can be expressed as

$$\frac{1}{\rho} = \frac{M_s}{E_s I_s}, \tag{3}$$

where E_s represents the elastic modulus of the beam and I_s represents the section moment of inertia.

Notably, the piezoelectric constitutive equation can be expressed as [14]:

$$\sigma_{px} = E_p\left(\varepsilon_{px} - d_{31}E_e\right), \tag{4}$$

where E_p stands for the elastic modulus of the piezoelectric patch, d_{31} is the piezoelectric constant, E_e stands for the strength of an electric field around the piezoelectric patch, σ_{px} stands for the stress of the piezoelectric patch, and ε_{px} stands for the strain of the piezoelectric patch, respectively. The piezoelectric patches are assumed as very thin, consequently σ_{px} and ε_{px} can be constant. No change occurs to the neutral layer of the beam after the piezoelectric patch is attached to the beam surface. The strain of the piezoelectric patch along the x direction is equal to the strain of the beam on the upper surface as follows:

$$\varepsilon_{px} = \varepsilon_s. \tag{5}$$

For ease of calculations, it is assumed that the neutral layer of the beam does not change while the thickness of the piezoelectric patch cannot be ignored. Accordingly, the bending moment of the piezoelectric patch can be written as

$$M_p = b\int_{H/2}^{(H/2)+h} \sigma_{px} z dz = b\int_{H/2}^{(H/2)+h} E_p\left(d_{31}E_e - \frac{z}{\rho}\right) z dz, \tag{6}$$

where h represents the thickness of the piezoelectric patch and M_p represents the bending moment of the piezoelectric patch. M_p and M_s refer to the relationships between internal forces, which can be expressed as

$$M_p = -M_s. \tag{7}$$

Finally, by assembling equations (1), (2), (3), (4), (5), (6) and (7), the trailing-edge deflection angle can be calculated by the following equation:

$$\beta = \frac{1}{1 + (2h/H) + \left(4h^2/3H^2\right) + \left(A_s E_s / 3A_p E_p\right)} \cdot d_{31} U\left(\frac{1}{H} + \frac{1}{h}\right) \cdot \frac{2l_2}{H}. \tag{8}$$

As to the aerodynamic calculation, the thin-airfoil camberline is divided into n distributed subpanels where the piezoelectric trailing edge is equally divided into n_2 distributed subpanels and the other part is equally divided into n_1 distributed subpanels. It is notable that the trailing

edge deflection angle and piezoelectric voltage are linearly dependent; accordingly, a discrete expression of equation (8) is defined as

$$\beta_i = K_{\mathrm{p}i} U, \tag{9}$$

where

$$K_{\mathrm{p}i} = \begin{cases} 0, & 1 \le i \le n_1, \\ \dfrac{1}{1 + (2h/H) + \left(4h^2/3H^2\right) + \left(A_{\mathrm{s}}E_{\mathrm{s}}/3A_{\mathrm{p}}E_{\mathrm{p}}\right)} \cdot d_{31}\left(\dfrac{1}{H} + \dfrac{1}{h}\right) \cdot \dfrac{2l_2(i-n_1)}{Hn_2}, & n_1 + 1 \le i \le n_1 + n_2. \end{cases} \tag{10}$$

2.3. Aerodynamic Force Calculation of Morphing Wing. The present study considers the aerodynamic force of the 2D wing as a thin airfoil with a significantly different configuration, regardless of the actual conditions of its airfoil. The position vector of the camberline can be expressed as a parametric equation as follows:

$$\mathbf{r} = x(s)\mathbf{e}_X + y(s)\mathbf{e}_Y, \tag{11}$$

where $\mathbf{e}_X$ and $\mathbf{e}_Y$ are the basis of X-0-Y.

The expressions of the total aerodynamic lift L and the total aerodynamic moment M are as follows [15]:

$$\begin{cases} L = qS\displaystyle\int_0^l C_{\mathrm{p}} \frac{dx(s)}{ds} ds = qS \int_0^l C_{\mathrm{p}} \cos\varphi ds, \\ M = \displaystyle\int_0^l qSC_{\mathrm{p}} \left(\frac{d\mathbf{r}}{ds} \times (\mathbf{r} - \mathbf{r}_0)\right) ds = qS \int_0^l C_{\mathrm{p}}((x(s) - x_0)\cos\varphi + (y(s) - y_0)\sin\phi)\varphi ds, \end{cases} \tag{12}$$

where q represents the dynamic pressure around the wing, S represents the reference wing area, C_{p} represents the aerodynamic pressure coefficient distribution at s, x_0 and y_0 represent the coordinates of the positions of the torsion spring, and φ represents the local downwash angle.

VLM is a numerical method for solving the steady aerodynamic loads of a 2D wing. Herein, the thin-airfoil camberline is divided into n equally distributed subpanels, and the n vortex points are placed at the quarter-chord point of each panel. Accordingly, the aerodynamic force can be written as

$$\begin{cases} L = \displaystyle\sum_{i=1}^{n} qSC_{\mathrm{p}i} \cos\varphi_i \Delta s_i, \\ M = \displaystyle\sum_{i=1}^{n} qSC_{\mathrm{p}i} \cdot ((x_i - x_0)\cos\varphi_i - (y_i - y_0)\sin\varphi_i)\Delta s_i, \end{cases} \tag{13}$$

where $C_{\mathrm{p}i}$ represents the aerodynamic pressure coefficient distribution at the ith panel. Δs_i represents the length of the ith panel, and φ_i represents the local downwash angle. The aerodynamic force obtained by equation (13) is based on the real aerodynamic shape considered as the aerodynamic force obtained by the geometrically exact VLM in this context.

When the traditional linear VLM is used in aeroelastic analysis, the aerodynamic force is independent of the local downwash angle. The aerodynamic solution formula of traditional linear VLM can be simplified by equation (13) as

$$\begin{cases} L = \displaystyle\sum_{i=1}^{n} qSC_{\mathrm{p}i} \Delta s_i, \\ M = \displaystyle\sum_{i=1}^{n} qSC_{\mathrm{p}i} \cdot (x_i - x_0)\Delta s_i. \end{cases} \tag{14}$$

In addition to the difference in the aerodynamic solution formula, the difference between the two VLMs is also reflected in the solution of pressure coefficient distribution.

When the aerodynamic force is calculated by traditional linearized VLM, the aerodynamic influence coefficient matrix is regarded as constant. Besides, the boundary conditions are linearized. Consequently, the aerodynamic forces mentioned above are linear, whose coefficients are constant. The C_{p} can be defined in equation (15) [15] as follows:

$$\begin{pmatrix} C_{\mathrm{p}1} \\ \vdots \\ C_{\mathrm{p}N} \end{pmatrix} = -\frac{2n}{l} A_0^{-1} \begin{pmatrix} \alpha + \theta + \beta_1 \\ \vdots \\ \alpha + \theta + \beta_n \end{pmatrix}, \tag{15}$$

where A_0 denotes the aerodynamic influence coefficient matrix before deformation.

Substitute equation (15) into equation (14), and we can obtain

$$\begin{cases} L = -2qSWA_0^{-1}N^T, \\ M = -2qSD_0A_0^{-1}N^T, \end{cases} \tag{16}$$

where $N = [\alpha + \varphi_1, \cdots, \alpha + \varphi_n]$, $\varphi_i = \theta + \beta_i$, $W = [1, \cdots, 1]$, $D_0 = [d_1, \cdots, d_N]$, and d_i denotes the distance from the center of the ith panel to the torsion spring before deformation.

It can be seen from equation (16) that there is a linear relationship between the airfoil pitch angle θ and the aerodynamic moment. So the traditional linearized VLM is very efficient in terms of analyzing the aeroelastic characteristic of the morphing piezoelectric wing. But its accuracy is still inadequate, which is demonstrated in the following two aspects. Firstly, the influence coefficient matrix of the aerodynamic force cannot reflect the influence of the trailing edge control surface. Secondly, the real boundary conditions are not implemented where α and sin α are considered as equivalent. In order to offset the deficiencies, the geometrically exact VLM is proposed to calculate the aerodynamic forces of morphing wings.

The calculation of the pressure coefficient of the morphing piezoelectric wing by virtue of the geometrically exact VLM is as follows:

$$\begin{pmatrix} C_{\mathrm{p}1} \\ \vdots \\ C_{\mathrm{p}N} \end{pmatrix} = -\frac{2n}{l}A(U)^{-1}\begin{pmatrix} \sin(\alpha_0 + \theta + \beta_1) \\ \vdots \\ \sin(\alpha_0 + \theta + \beta_N) \end{pmatrix}, \tag{17}$$

where $A(U)$ denotes the influence coefficient matrix of the aerodynamic force which is a matrix function of piezoelectric voltage. This matrix function represents the relationship between wing deformation and influence coefficient matrix.

Substitute equation (17) into equation (13), the aerodynamic lift and moment are shown as

$$\begin{cases} \bar{L} = -2qS\bar{W}A(U)^{-1}\left(N + \widehat{N}\right)^T, \\ \bar{M} = -2qS\bar{D}A(U)^{-1}\left(N + \widehat{N}\right)^T, \end{cases} \tag{18}$$

where $\widehat{N} = [\widehat{\varphi}_1, \cdots, \widehat{\varphi}_n]$, $\widehat{\varphi}_i = -(1/6)(\alpha_0 + \varphi_i)^3 + o^3(\alpha_0 + \varphi_i)$, $\bar{W} = [\cos\varphi_1, \cdots, \cos\varphi_n]$, and $\bar{D} = [d_1 \cos\theta, \cdots, d_N \cos\theta]$.

Figure 2 shows the different discrete vortex representations of the morphing wing after deformation using different VLMs. At this phase, the camberline is divided into n subpanels, whose length is Δs_i. In Figure 2(a), the blue line represents the actual aerodynamic surface before deformation. And the red line represents the real aerodynamic surface after deformation. In Figures 2(b) and 2(c), the dots represent the vortex points and the forks represent the control points. The vector $\mathbf{n}_i$ is the normal vector of the ith panel in the aerodynamic surface after deformation which represents the zero normal flow boundary condition. It can be seen from Figures 2(b) and 2(c) that when the aerodynamic force is calculated by the traditional linear VLM in the presence of deformation of the aerodynamic surface, the positions of the control point and vortex point remain unchanged, and only the boundary condition is changed. When the geometrically exact VLM is employed to calculate the aerodynamic force, the position of the control point and my point will be changed correspondingly with the deformation of the aerodynamic surface. Obviously, it can be seen that the vortex distribution points change significantly when the trailing-edge deflects, so the aerodynamic influence coefficient matrix calculated by VLM cannot be considered as constant.

2.4. Aeroelastic Analysis Using Traditional Linearized VLM. The morphing piezoelectric wing balance equation is defined as follows:

$$M = K_\theta\theta. \tag{19}$$

Based on equations (16) and (19), when the system is in a state of equilibrium, the pitch angle of the airfoil $\theta*$ can be obtained as follows:

$$\theta^* = \frac{-2qSD_0A_0^{-1}\left(\alpha W^T + UK_{\mathrm{P}}^T\right)}{K_\theta + 2qSD_0A_0^{-1}W^T}, \tag{20}$$

where $K_{\mathrm{P}} = [K_{\mathrm{p}1}, \cdots K_{\mathrm{p}N}]$.

The denominator of equation (20) will become zero when the dynamic pressure reaches a certain value, which makes $\theta*$ approach infinity and the 2D wing becomes unstable. The certain dynamic pressure is denoted by divergent dynamic pressure q_{div}. It is a crucial aeroelastic parameter for the wing in that it represents the highest dynamic pressure that the wing can sustain before being destroyed. The q_{div} can be obtained by the following equation using traditional linearized VLM:

$$q_{\mathrm{div}} = \frac{K_\theta}{-2SD_0A_0^{-1}W^T}. \tag{21}$$

It can be seen from equation (21) that the divergent dynamic pressure calculated by traditional linearized VLM is proportional to K_θ and is related to the aerodynamic arm D_0. Therefore, increasing the torsional stiffness of the wing or reducing the aerodynamic arm can both improve q_{div}.

The downward deflection of the control surface increases the lift while it produces a negative pitching moment, which makes the 2D wing rotate in the direction of reducing the angle of attack, thereby diminishing the control surface efficiency. The efficiency keeps decreasing with the increase of the dynamic pressure, which even leads to aileron reversal. Aileron reversal is defined as the concurrence of the increase of the trailing edge deflection angle and the decrease of the total lift.

Considering that the airfoil rotated under the aerodynamic load, the lift is given by

$$L_\theta = \frac{L_0K_\theta - L_0(\partial M/\partial\theta) + M_0(\partial L/\partial\theta)}{K_\theta - (\partial M/\partial\theta)}, \tag{22}$$

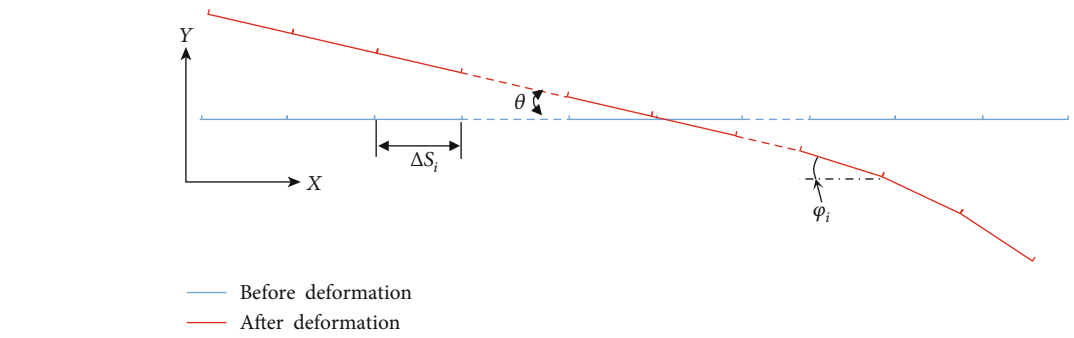

(a) Aerodynamic surface before and after deformation

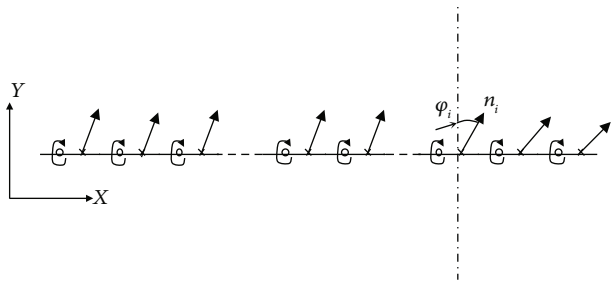

(b) Discrete vortex representation using traditional linear VLM

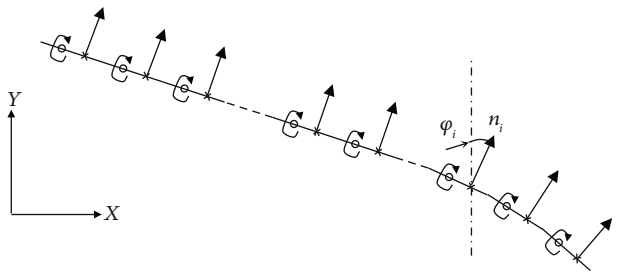

(c) Discrete vortex representation using geometrically exact VLM

FIGURE 2: The different discrete vortex representations using different VLMs.

where L_0 and M_0 represent the aerodynamic lift and moment prior to aeroelastic deformation which can be obtained by equation (16) when θ is set to zero.

When the lift becomes zero, the control surface fails to work, thus the efficiency of the control surface is reduced to zero. The dynamic pressure in the presence of control reversal is called the control reversal dynamic pressure, denoted by q_R. When the numerator of equation (22) is set as zero, we substitute equations (16) and (21) into equation (22) to obtain q_R, which is written as

$$q_R = \frac{DA_0^{-1}\left(W^T + UK_P^T\right)K_\theta}{2SD_0A_0^{-1}UK_P^TWA_0^{-1}W^T - 2SD_0A_0^{-1}W^TWA_0^{-1}UK_P^T}. \tag{23}$$

Besides, the efficiency of the control surface is defined as the ratio of the aerodynamic lift after aeroelastic deformation to that before aeroelastic deformation, as in

$$\eta = \frac{L_\theta}{L_0} = 1 + \frac{-2qsWA_0^{-1}W^T}{K + 2qsD_0A_0^{-1}W^T}\frac{D_0A_0^{-1}\left(UK_P^T + W^T\right)}{WA_0^{-1}\left(UK_P^T + W^T\right)}. \tag{24}$$

2.5. Aeroelastic Analysis Using Geometrically Exact VLM. The morphing piezoelectric wing balance equation using aerodynamic moments in equation (18) is defined as follows:

$$\bar{M} = K_\theta\theta. \tag{25}$$

It is worth noting that equation (25) is a nonlinear transcendental equation. In fact, equation (25) is an aeroelastic equation, whose nonlinearity appears in the process of structural and aerodynamic coupling. Although VLM is a linear aerodynamic method, the relationship between aerodynamic moment and pitch angle θ obtained by the geometrically accurate VLM is not linear through the analysis in Section 2.4.

Through the following equations, we can obtain the pitch angle θ of the 2D wing in balance through an iterative solution, as in

$$\theta_{n+1} = \theta_n - \frac{\bar{M}(\theta_n) - K_\theta\theta_n}{\left(\partial\bar{M}/\partial\theta\right)|_{\theta=\theta_n} - K_\theta}. \tag{26}$$

There is some difference in the static aeroelastic stability of the 2D wing between the use of the geometrically exact VLM and traditional linearized VLM. Because unlike equation (19), equation (25) has multiple solutions in some conditions, which warrants analysis of the stability of each solution. According to the energy criterion [16], the 2D wing is in a stable equilibrium state when the variation of elastic potential energy is less than the variation of aerodynamic work in the presence of a slight disturbance. Besides, when the variation of elastic potential energy is equal to the variation of aerodynamic work in the presence of a slight disturbance, the system is in a critical equilibrium state while the corresponding aerodynamic load is a critical load.

Under a slight disturbance of the pitch angle $\delta\theta$, the variation of aerodynamic work can be defined as follows:

$$\Delta W_a = \int_{\theta^*}^{\theta^*+\delta\theta} \bar{M}(\theta)d\theta = \bar{M}(\theta^*)\delta\theta + \left.\frac{\partial\bar{M}}{\partial\theta}\right|_{\theta=\theta^*}\theta^*\delta\theta + \frac{1}{2}\left.\frac{\partial\bar{M}}{\partial\theta}\right|_{\theta=\theta^*}\delta\theta^2. \tag{27}$$

And the variation of spring elastic potential energy can be defined as

$$\Delta U = \frac{1}{2} K_\theta \delta\theta^2 + K_\theta \theta^* \delta\theta. \tag{28}$$

When $\Delta U = \Delta W_a$, the system is in neutral equilibrium. Applying equations (27) and (28) to it, the following simplified critical equilibrium state is reached:

$$\left.\frac{\partial \bar{M}}{\partial \theta}\right|_{\theta=\theta^*} = K_\theta. \tag{29}$$

Traditional aeroelastic analysis is based on linear aerodynamic theory. As a result, the critical equilibrium solution of the linear 2D wing system can be obtained as the divergence dynamic pressure. However, when using the geometrically exact VLM, the 2D wing system becomes nonlinear. Thus, it becomes inappropriate to discuss the divergence dynamic pressure of the nonlinear system. Instead, the number and stability of equilibrium solutions should be analyzed. Due to the complexity of solving equation (25), the numerical solution of the static aeroelastic stability of the piezoelectric wing is obtained for theoretical analysis instead of the analytical solution.

There is also some difference between the control surface efficiency of the 2D wing by the geometrically exact VLM and that by the traditional linearized VLM. Unlike the linear solution, the aerodynamic forces are related to the pitch angle θ and the trailing edge deflection angle β. Therefore, it is inappropriate to define control reversal dynamic pressure when aerodynamic lift reaches 0. Instead, the control reversal occurs when the lift decreases with the increase of β, and the corresponding dynamic pressure is called reverse dynamic pressure q_r which can be obtained by the following equation:

$$\left.\frac{\partial \bar{L}}{\partial U}\right|_{\theta=\theta^*} = 0. \tag{30}$$

Also, the control surface efficiency is defined similar to equation (22) as

$$\eta = \frac{\bar{L}}{\bar{L}_0}. \tag{31}$$

In this study, both equations (30) and (31) were solved by the nonlinear equation solution function of the MATLAB R2014a software.

3. Numerical Validation

In this paper, the piezoelectric constant d_{31} is always set to be $3.85 \times 10^{14} V \cdot m/N$ and all the structure parameters are listed in Table 1. The parameters of the piezoelectric patch are determined by real MFC.

In addition, the traditional wing with a rigid trailing edge is introduced to compare with the morphing piezoelectric wing. These two wings have the same chord length of control surface and the same vertical displacement of the trailing edge, as shown in Figure 3. Both the wings are considered to have the equivalent deflection angle, β.

3.1. Aerodynamic Characteristics of the Morphing Piezoelectric Wing. The aerodynamic loads of the morphing piezoelectric wing were calculated by both traditional linearized VLM and geometrically exact VLM. The lift coefficient and the moment coefficient with respect to the angle of attack are plotted in Figure 4. The angles of attack range from 0° to 12°. The torsion spring is set at 35% of chord-wise length and the control surface is 30% of chord. According to equation (8), the trailing edge of the morphing piezoelectric wing is deflected by 3.585 degrees per kilovolt.

It can be seen from Figure 4 that at the same angle of attack, the greater the driving voltage, the greater the aerodynamic force and the smaller the aerodynamic moment. The reason behind this is that a greater driving voltage creates a larger deflection of the trailing edge which leads to a bigger increment of angle of attack at the trailing edge, while the aerodynamic lift increased with the angle of attack. However, it shortens the mean aerodynamic chord of the wing, which makes the trailing edge deflect downward at greater driving voltage, resulting in the decrease of the aerodynamic moment. This conclusion is consistent with both traditional linearized VLM and geometrically exact VLM.

In addition, although the aerodynamic lifts and moments increase with the angle of attack, a slight difference exists between these two VLMs. For one thing, when the angle of attack α ranges from 0° to 6°, the aerodynamic coefficient calculated by the two VLMs are almost the same. In contrast, when α is above 6°, C_l and C_m calculated by the geometrically exact VLM are smaller than those calculated by the traditional linearized VLM. For another, with the increase of α and driving voltage, the differences between the two aerodynamic coefficients become larger, which is mainly attributed to the limitation of the traditional linearized VLM. When the 2D wing has a large angle of attack or a large trailing edge deflection angle, the boundary conditions cannot be linearized and the corresponding aerodynamic influence coefficient matrix cannot be considered as a constant matrix. As a result, the traditional linearized VLM is inapplicable for analyzing the aerodynamic characteristics of the 2D wing in this context. In contrast, the geometrically exact VLM exhibits considerable accuracy in calculating the aerodynamic coefficients at a large angle of attack and the trailing edge deflection angle. Results are consistent with the aerodynamic characteristics of the thin airfoil.

Consequently, a case is set to explore the influence of control surface length on aerodynamic coefficients. With the angle of attack kept as 0° and the equivalent deflection angle ($\beta = 7.17°$) of the different trailing edge unchanged, the starting location of the control surface was changed to calculate the aerodynamic coefficient. The results are shown in Figure 5.

Figure 5 shows that as the starting location of the control surface moves backward, the lift coefficient and moment coefficient caused by the trailing edge deflection decrease, which can be attributed to the lowered effective area of the

Table 1: Geometric parameters of the wing and the piezoelectric patch.

	Modulus of elasticity (Gpa)	Length (mm)	Width (mm)	Height (mm)
Rigid part of the wing	—	700	—	—
Elastic bending part of the wing	200	300	36	1.5
Piezoelectric patch	74	300	36	1

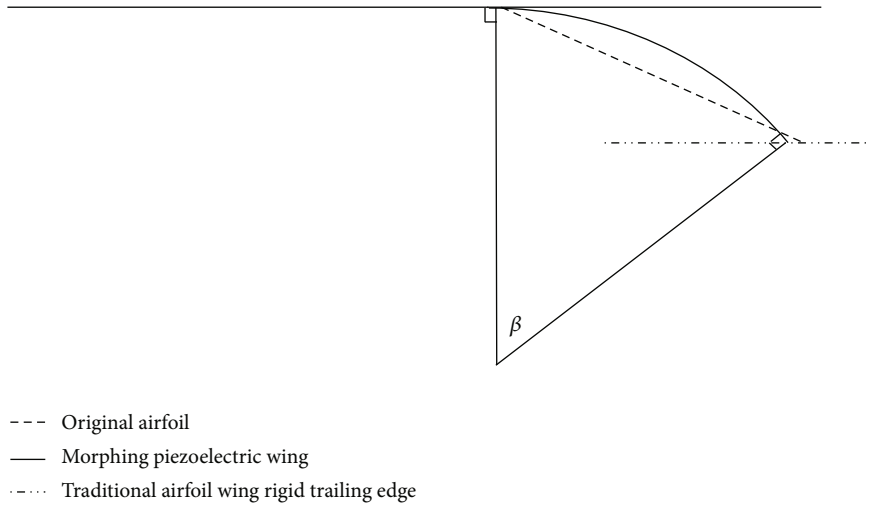

Figure 3: Wings with the equivalent deflection angle.

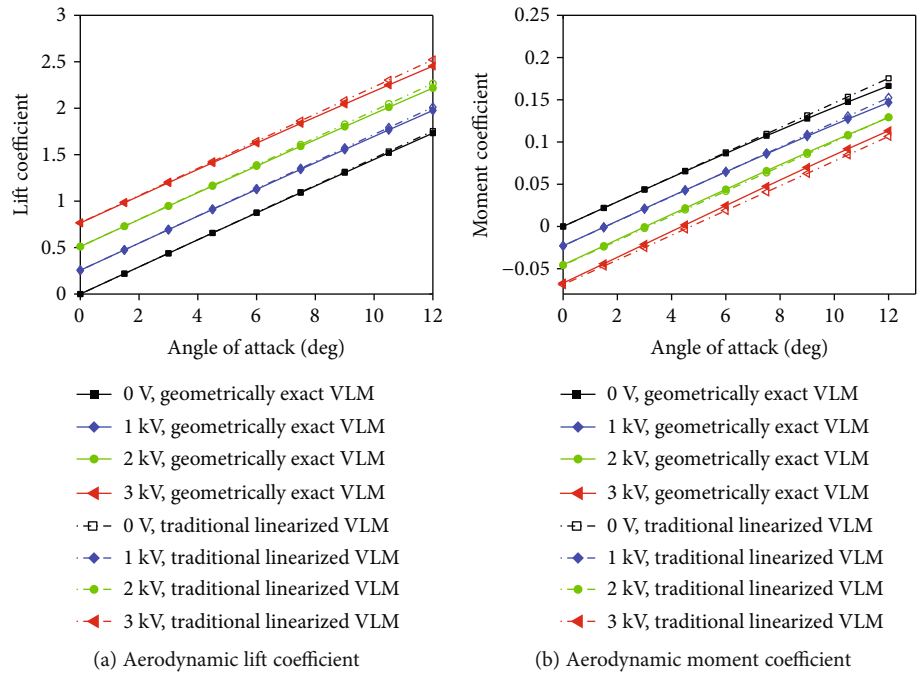

(a) Aerodynamic lift coefficient (b) Aerodynamic moment coefficient

Figure 4: Effect of angle of attack and driving voltages on aerodynamic coefficient.

control surface. In addition, both C_l and C_m obtained by the geometrically exact VLM are smaller than those obtained by the traditional linearized VLM, which is consistent with the above conclusion. In Figure 5(a), the C_l of the morphing piezoelectric wing is higher than that of the wing with a rigid trailing edge. According to Figure 5(b), the aerodynamic moment of the morphing piezoelectric wing is higher than that of the traditional wing. Concurrently, the moment peaks when the starting location of control surface is around 70% chord. Besides, the C_m of the traditional wing with a rigid trailing edge airfoil decreases monotonically with the starting location going backward. It can be concluded that the

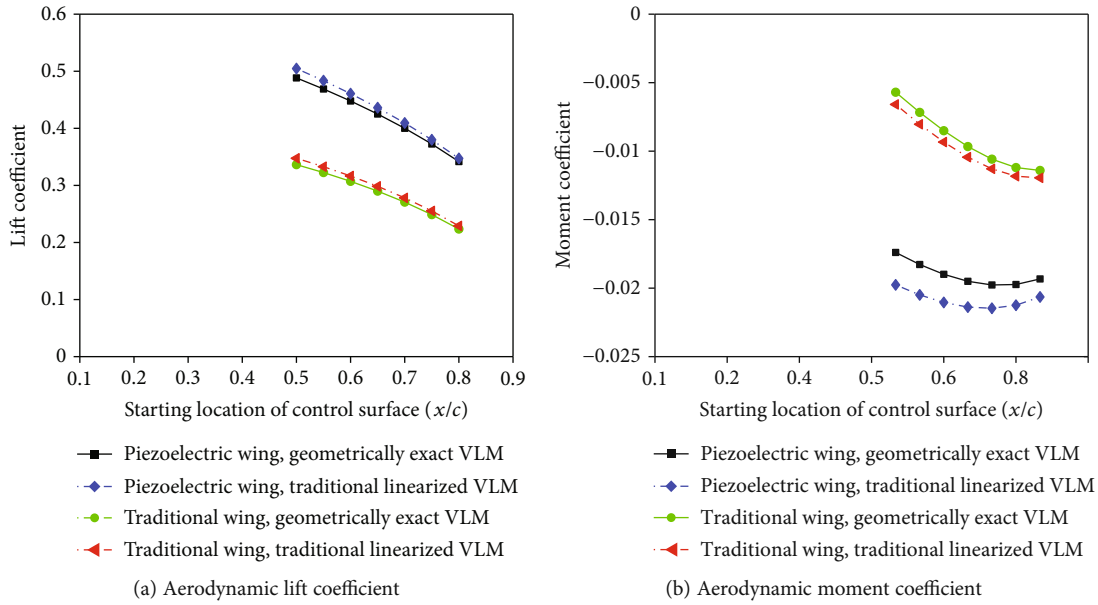

(a) Aerodynamic lift coefficient (b) Aerodynamic moment coefficient

Figure 5: Effects of control surface length on aerodynamic coefficient.

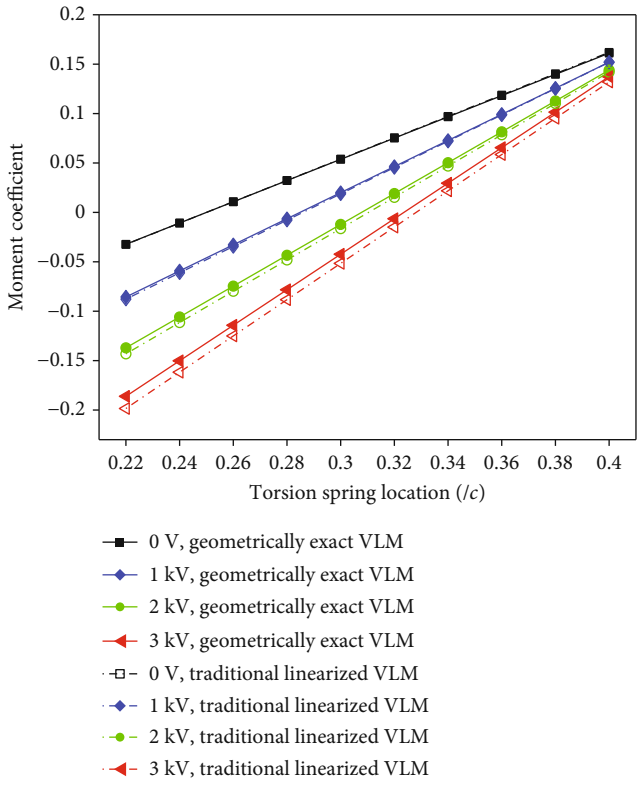

Figure 6: Effects of torsion spring location and driving voltages on aerodynamic moment.

morphing piezoelectric wing has a larger lift coefficient and a larger negative pitching moment coefficient than the traditional wing with the same trailing edge deflection.

The chord-wise location of the torsion spring also has an effect on the aerodynamic moment versus piezo actuation. Another case is planned to research it. In this case, the two VLMs are used to calculate the aerodynamic moment of the morphing piezoelectric wing with different voltage and torsion spring locations at 5° angle of attack. The result is shown in Figure 6.

As Figure 6 illustrates, the aerodynamic moment increases as the torsion spring location moves backwards. Furthermore, the aerodynamic moment obtained by the geometrically exact VLM is larger than that obtained by the traditional linear VLM under the same driving voltages. This is because the geometrically exact VLM can fully consider the influence of the change of the downwash angle and aerodynamic arm caused by the wing deformation on the aerodynamic moment, while the traditional linear VLM ignores this point. It is worth noting that, the aerodynamic moments calculated by the two VLMs are the same at 0 driving voltage and the aerodynamic moments are 0 at the quarter-chord length. This can be interpreted that the camberline of the morphing piezoelectric wing is a straight line at 0 driving voltage whose aerodynamic center is also located at a quarter-chord length.

3.2. Aerodynamic Load Redistribution of Morphing TE Wing. In this section, different wings are considered and their properties are listed in Table 2 in order to investigate the effects of aeroelastic deformation on the changes of aerodynamic loads. The aerodynamic load redistribution is then plotted in Figure 7 and the overall lifts using the traditional linearized VLM or the geometrically exact VLM are listed in Table 3.

As shown in Figure 7(a), the airfoil without a control surface rotates upward under the current aerodynamic load resulting in an increase (3.2°) of the angle of attack. Thus, the overall aerodynamic lifts increase under an aeroelastic effect. Figure 7(b) shows the aerodynamic load distribution of the morphing piezoelectric wing. Due to the deflection of

Table 2: Properties of different airfoils.

	l_2 (/c)	l_0 (/c)	K_θ (N·m/rad)	q (Pa)	α (deg)	β (deg)
Airfoil without control surface	—	0.33	10	200	5	—
Morphing piezoelectric wing	0.3	0.33	10	200	5	10
Traditional wing with rigid trailing edge	0.3	0.33	10	200	5	10

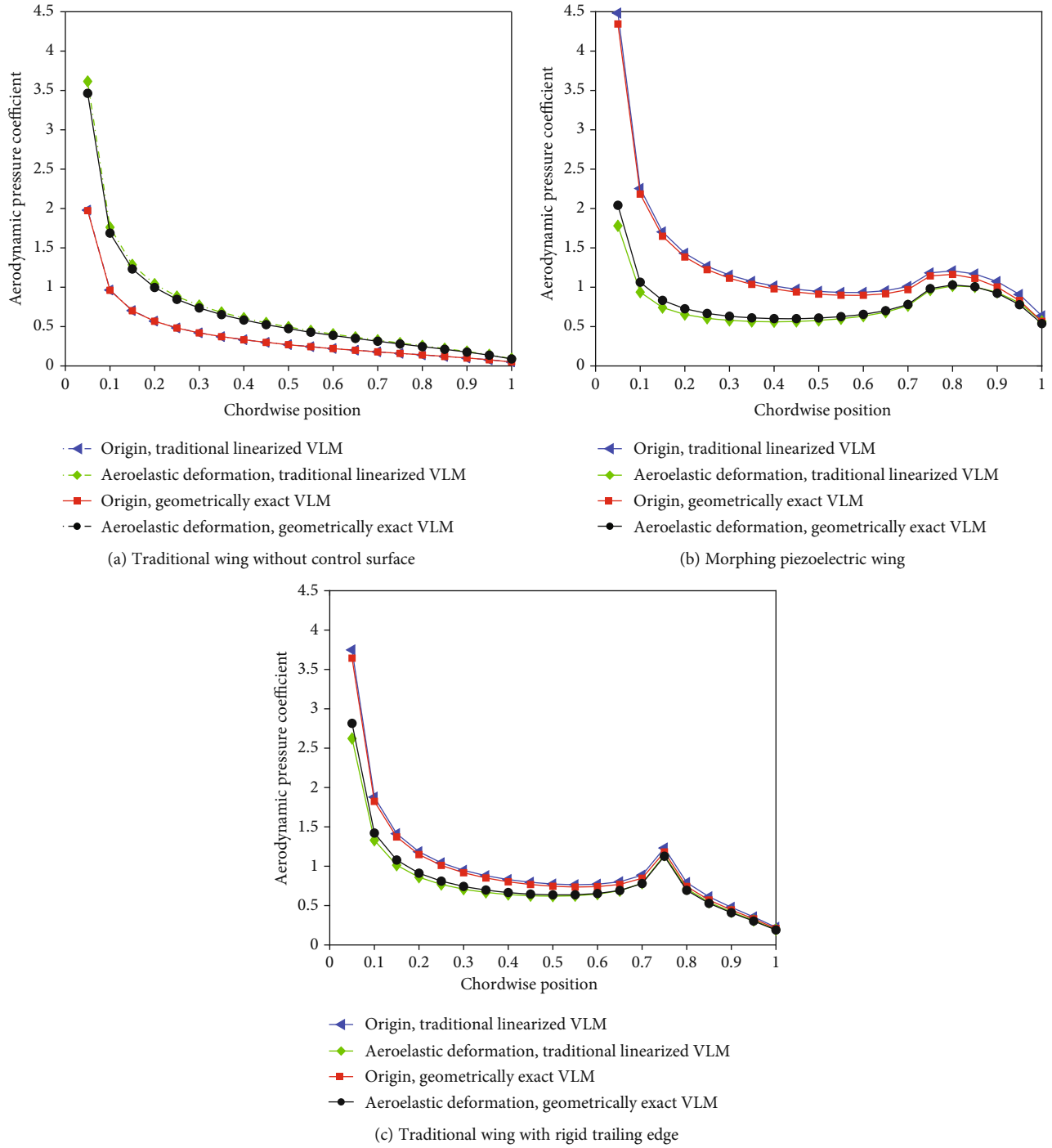

(a) Traditional wing without control surface

(b) Morphing piezoelectric wing

(c) Traditional wing with rigid trailing edge

Figure 7: Aerodynamic load redistribution after aeroelastic deformation.

Table 3: Total aerodynamic lift.

	Airfoil without control surface	Morphing piezoelectric wing	Traditional wing with rigid trailing edge
Origin, traditional linearized VLM	3.5793	11.3167	9.9551
Origin, geometrically exact VLM	3.2547	10.8865	9.4613
Aeroelastic deformation, traditional linearized VLM	6.1865	8.5917	7.8819
Aeroelastic deformation, geometrically exact VLM	5.9250	8.9471	8.1935

the trailing edge, the aerodynamic load on the trailing edge is significantly increased. When it comes to the aeroelastic effect, the airfoil rotates downward under aerodynamic load, bringing about a decrease of overall aerodynamic lift. The reason is that when the trailing edge deflected downward, it generated a negative pitching moment which decreased the angle of attack. Figure 7(c) shows the aerodynamic load distribution of the traditional wing with a rigid trailing edge, in which the aerodynamic load sees a sudden change at the start point of the rigid trailing edge. This is because the additional angle of attack is noncontinuous when the trailing edge deflects downward, and the airfoil also rotated downward under aerodynamic load, as in Figure 7(b).

Table 3 indicates that with the same equivalent deflection angle ($\beta = 10^\circ$), the lift coefficient of the morphing piezoelectric wing is higher than that of the traditional wing. Furthermore, aeroelastic deformation is demonstrated to significantly change the lift coefficient. Moreover, at the same trailing edge rotation angle, the negative pitching moment of the morphing piezoelectric wing is larger than that of the traditional wing. As a result, the C_l of the morphing piezoelectric wing declines to a larger extent than that of the traditional wing. Notably, the origin lift calculated by the geometrically exact VLM is 4% lower than the lift calculated by the traditional linearized VLM. This is because the induced velocity in the traditional linearized VLM is larger than that in the geometrically exact VLM. In contrast, the lift calculated by the geometrically exact VLM is larger than the lift calculated by the traditional linearized VLM as a result of aeroelastic deformation when the trailing edge deflected downward. This is because the aeroelastic pitch angle calculated by the geometrically exact VLM is smaller, which leads to a larger angle of attack in this case.

3.3. Static Aeroelastic Stability of Morphing TE Wing. In this section, some cases are set to reflect the influence of the angle of attack, trailing edge deflection angle, trailing edge deflection mode, and torsion axis location on the static aeroelastic stability of the morphing TE wing using the geometrically exact VLM. In this section, the parameters of the morphing piezoelectric wing and the traditional wing with a rigid trailing edge are set as the same as those in Section 3.2. The relationship between dynamic pressure and airfoil pitch angle θ of the piezoelectric morphing wing is obtained under different conditions, which are shown in Figure 8. In addition, q_{div} is the diverging dynamic pressure of the wing in the current state calculated by the traditional linear VLM. The x-axis of Figure 8 is the ratio of dynamic pressure to divergence dynamic pressure q_{div} using the traditional linearized VLM, and the y-axis is the pitch angle θ. The solid lines represent stable solutions, while the dotted lines represent unstable solutions.

Figure 8(a) shows the equilibrium state of a 2D wing with a 0° angle of attack and a 0° trailing edge deflection angle. The solution of the equilibrium state is achieved by solving the nonlinear transcendental equation, as in equation (25). It can be seen that when the dynamic pressure is less than q_{div}, the equilibrium equation has only one stable solution. This indicates that the 2D wing is in static stability in this situation. Nevertheless, when dynamic pressure is greater than q_{div}, there are three solutions to the equilibrium with the same dynamic pressure: (1) a stable solution with a pitch angle of more than 0°; (2) a stable solution with a pitch angle of less than 0°; and (3) an unstable solution with a pitch angle of 0°. This is a typical static bifurcation of a nonlinear system and is part of pitchfork bifurcation. The bifurcation value is q_{div}. This indicates that the zero solution of the nonlinear 2D wing system is consistent with the linear condition. The final position of the 2D wing depends on the disturbance.

Figures 8(b)–8(d) show the equilibrium states of the 2D wing with varying angles of attack and 0° trailing edge deflection angle. In the case of Figure 8(b), the angle of attack is set as 1°. Figure 8(b) shows that only when the dynamic pressure is less than q_{div} can the system achieve a stable equilibrium solution with a positive pitch angle. When the dynamic pressure exceeds q_{div}, saddle knot bifurcation occurs in the system. In this context, there are three solutions when the original equilibrium solution maintains nonlinear development. There are two new equilibrium solutions with a negative pitch angle. The one with a smaller pitch angle is unstable and is referred to as saddle point, while the other is stable and is referred to as stable knot. In addition, the bifurcation value is 1.115 q_{div}. In the case of Figure 8(c), the angle of attack is set as 5°. Figure 8(c) shares the same topology with Figure 8(b). But its bifurcation value is 1.3563 q_{div}. In the case of Figure 8(d), the angle of attack is set as -1°. Figures 8(d) and 8(b) are mirror images of the x-axis and share the same bifurcation value. It can be concluded that by means of the geometrically exact VLM, the angle of attack has a great impact on the static stability of the 2D wing, which is mainly embodied in three aspects. Firstly, a nonzero angle of attack changes the type of bifurcation diagram of the system. Secondly, the bifurcation value increases along with the increase of the angle of attack. Thirdly, the sign of the angle of attack is independent of the bifurcation value.

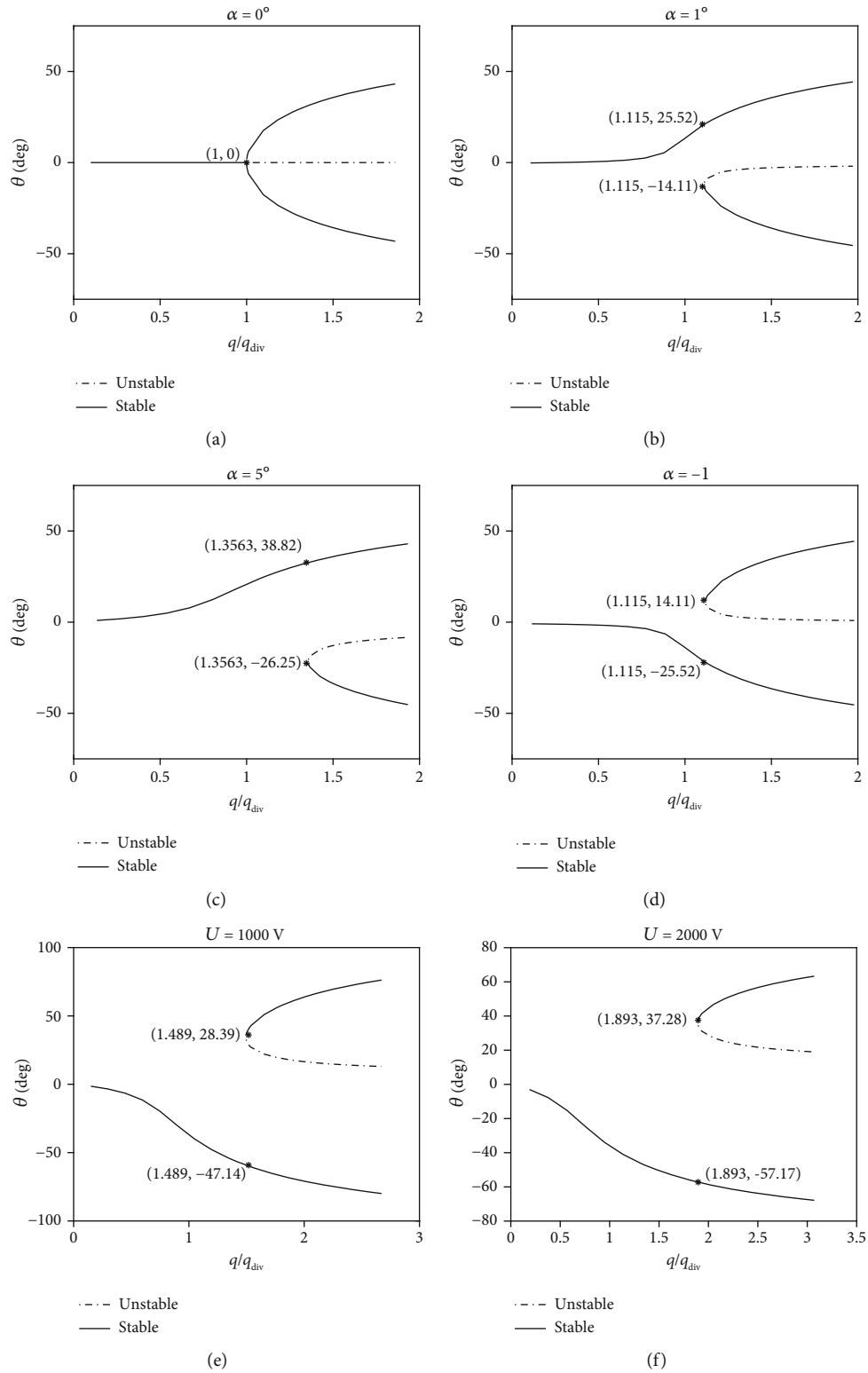

Figure 8: Continued.

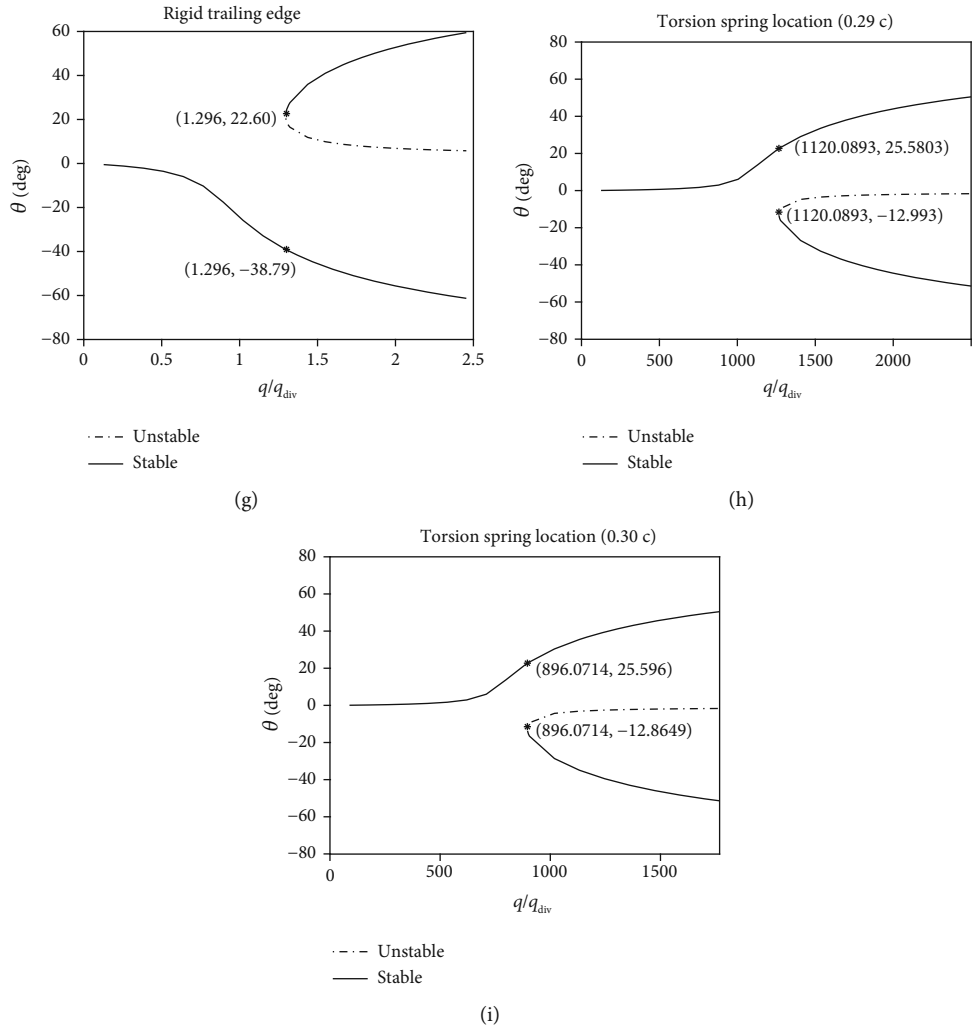

Figure 8: Relationship between dynamic pressure and pitch angle θ in equilibrium state using the geometrically exact VLM.

Figure 8(e) shows the equilibrium state of the morphing piezoelectric wing with a 0° angle of attack and a 1000 V piezoelectric voltage which generates a 4.88° trailing edge deflection angle. It can be seen that the topology of the bifurcation diagram is the same as the one with a negative angle of attack. Meanwhile, the bifurcation value is 1.489 q_{div}. Figure 8(f) shows the equilibrium state of the morphing piezoelectric wing with a 0° angle of attack and a 2000 V piezoelectric voltage which generates a 9.76° trailing edge deflection angle. Likewise, the topology of the bifurcation diagram is the same as that of Figure 8(e) but the bifurcation value increases to 1.893 q_{div}. It can be concluded that the bifurcation value increases along with the trailing edge deflection angle. This can be attributed to the fact that the trailing edge deflection downward causes a negative pitching moment on the 2D wing, which is similar to the wing with a negative angle of attack. Figure 8(g) shows the equilibrium state of the traditional wing with a rigid trailing edge with a 0° angle of attack and a 4.88° trailing edge deflection angle. The topology of Figure 8(g) is the same as that of Figure 8(e), but the bifurcation value is reduced to 1.296 q_{div}. It can be concluded that bifurcation value increases along with the trailing edge deflection angle. Furthermore, the traditional wing with a rigid trailing edge has a smaller bifurcation value than the morphing piezoelectric wing with the same trailing edge deflection angle. This is because the morphing piezoelectric wing generates a larger negative pitching moment than the traditional wing. Similar to the previous conclusion, the morphing piezoelectric wing has a larger equivalent angle of attack which leads to a higher bifurcation value.

Figures 8(h) and 8(i) show the equilibrium states of the morphing piezoelectric wing with a 1° angle of attack and a 1000 V driving voltage at different torsion spring locations, 29% chord length (0.29c), and 30% chord length (0.3c). Figures 8(h) and 8(i) have the same topology of the bifurcation diagram which is similar to Figure 8(b) but with different bifurcation value. The bifurcation value (1120.09 Pa) in Figure 8(h) is larger than that (896.07 Pa) in Figure 8(i). This is because in the case of Figure 8(h), the torsion spring location is closer to the aerodynamic center which leads to a smaller aerodynamic arm. Under the same aerodynamic load, a small aerodynamic arm means a small aerodynamic moment, which makes the system difficult to bifurcate. Therefore, a reasonable arrangement of the torsion axis

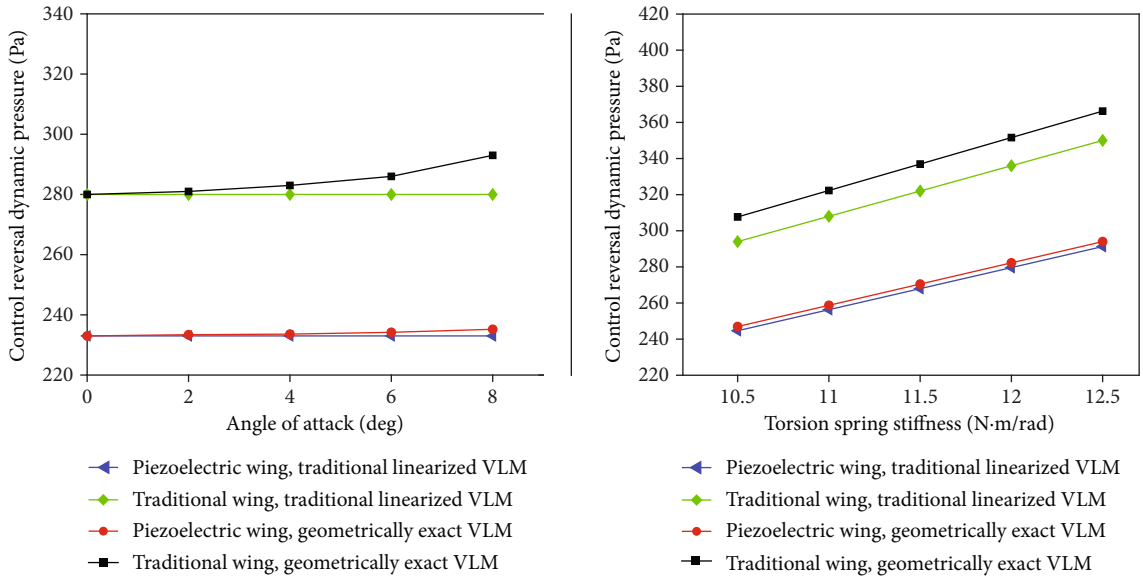

(a) Angle of attack vs. control reversal dynamic pressure

(b) Torsion spring stiffness vs. control reversal dynamic pressure

Figure 9: Factors related to the control reversal dynamic pressure.

location can significantly improve the bifurcation value by reducing the aerodynamic arm of the wing.

In the numerical validation, it can be seen that there is always a solution in equation (25), indicating that there is no divergent dynamic pressure of the 2D wing using the geometrically exact VLM. This can be attributed to the fact that the aerodynamic moments cannot keep increasing with the pitch angle due to the decrease of the aerodynamic arm. But this does not mean that the wing can sustain a gigantic dynamic pressure since the wing has strength constraints and may be destroyed before it reaches equilibrium.

3.4. Control Reversal Dynamic Pressure of Morphing TE Wing. In this section, some cases with different angles of attack and torsion spring stiffness are set to identify the factors related to the control reversal dynamic pressure. The results are given in Figure 8. In this section, the parameters of the morphing piezoelectric wing and the traditional wing with a rigid trailing edge are set the same as those in the Section 3.2.

Figure 9(a) shows the effect of the angle of attack on the control reversal dynamic pressure. In Figure 9(a), it can be seen that the control reversal dynamic pressure calculated by the traditional linearized VLM is not related to the angle of attack, while the control reversal dynamic pressure calculated by the geometrically exact VLM increases with the angle of attack. The q_R of the traditional wing is 21% larger than that of the morphing piezoelectric wing, since the traditional wing has a lower negative pitching moment and a lighter impact on aeroelastic deformation than the morphing piezoelectric wing. Figure 9(b) illustrates that q_R increases along with the increase of the pitch stiffness of the airfoil. This is due to the fact that high pitching stiffness of the airfoil leads to smaller aeroelastic deformation in the same aerodynamic load, which results in higher control reversal dynamic pressure.

4. Conclusion

Morphing trailing-edge wings, which can change their shape during flights, have the potential to improve the aerodynamic characteristics of aircraft, which warrants aeroelastic analysis for the morphing TE wings. Committed to the static aeroelastic characteristics of the morphing TE wings, this paper has developed a static aeroelastic analysis method using the geometrically exact VLM which gives equal prominence to both efficiency and medium accuracy. Firstly, the morphing piezoelectric wing was chosen and analyzed as a typical and simple model for morphing TE wings, and the relationship between piezoelectric voltage and trailing-edge deflection was tested. Then, the paper has established a set of cases for aeroelastic analysis of morphing TE wings using the geometrically exact VLM and shed light on their nonlinear aeroelastic characteristics. Finally, a series of simulations with different aerodynamic conditions were carried out on both the morphing piezoelectric wing and the wing with a rigid trailing edge. This paper has only explored the mechanism of the morphing TE wing without achieving any precise and detailed design. Based on the existing calculation results, some important conclusions can be summarized as follows:

(1) This paper has demonstrated the influence of aerodynamic nonlinearity on the static stability of the 2D wing system using the geometrically exact VLM. The system does not show divergence but bifurcation. Besides, the angle of attack, trailing-edge deflection angle, trailing-edge deflection mode, and torsion axis location all affect the bifurcation value and topology of the bifurcation diagram. Although this conclusion is conditional due to the limitation of the geometrically exact VLM, a general conclusion can be attained

(2) The characteristics of this method are verified by numerical examples. The geometrically exact VLM is more accurate than the traditional linearized VLM in calculating aerodynamic forces of a 2D wing with control surface in aeroelastic analysis. The influences of angle of attack, trailing-edge deflection angle, among others on static aeroelastic characteristics are taken into consideration, which play a significant role in engineering

(3) A morphing wing is inarguably a fluid-solid and control coupling system. As a result, by taking aerodynamic, structure, and control coupling into account, the method used in this paper can serve as an effective basic tool for morphing wing analysis and design optimization owing to its accuracy, adequate calculation, and inheritability of traditional methods

Data Availability

The data used to support the findings of this study are available from the corresponding author upon request.

Conflicts of Interest

The authors declare that there is no conflict of interest regarding the publication of this paper.

References

[1] S. Barbarino, O. Bilgen, R. M. Ajaj, M. I. Friswell, and D. J. Inman, "A review of morphing aircraft," *Journal of Intelligent Material Systems and Structures*, vol. 22, no. 9, pp. 823–877, 2011.

[2] S. Kota, J. A. Hetrick, R. Osborn et al., "Design and application of compliant mechanisms for morphing aircraft structures," in *Smart Structures and Materials 2003: Industrial and Commercial Applications of Smart Structures Technologies*, pp. 24–34, San Diego, CA, USA, 2003.

[3] P. Boschetti, A. Amerio, and E. Cárdenas, "Aerodynamic performance as a function of local twist in an unmanned airplane," in *47th AIAA Aerospace Sciences Meeting including The New Horizons Forum and Aerospace Exposition*, p. 1481, Orlando, FL, USA, 2009.

[4] V. Wickramasinghe, Y. Chen, M. Martinez, F. Wong, and R. Kernaghan, "Design and verification of a smart wing for an extremely-agile micro-air-vehicle," in *50th AIAA/ASME/ASCE/AHS/ASC Structures, Structural Dynamics, and Materials Conference*, p. 2132, Palm Springs, CA, USA, 2009.

[5] O. Bilgen, K. B. Kochersberger, D. J. Inman, and O. J. Ohanian III, "Novel, bidirectional, variable-camber airfoil via macrofiber composite actuators," *Journal of Aircraft*, vol. 47, no. 1, pp. 303–314, 2010.

[6] H. Monner, J. Riemenschneider, S. Opitz, and M. Schulz, "Development of active twist rotors at the German Aerospace Center (DLR)," in *52nd AIAA/ASME/ASCE/AHS/ASC Structures, Structural Dynamics and Materials Conference*, p. 1824, Denver, CO, USA, 2011.

[7] A. Pankonien and D. J. Inman, "Experimental testing of spanwise morphing trailing edge concept," in *Active and Passive Smart Structures and Integrated Systems 2013*, p. 868815, San Diego, California, USA, 2013.

[8] O. J. Ohanian, C. Hickling, B. Stiltner et al., "Piezoelectric morphing versus servo-actuated MAV control surfaces," in *53rd AIAA/ASME/ASCE/AHS/ASC Structures, Structural Dynamics and Materials Conference*, p. 1512, Honolulu, Hawaii, 2012.

[9] O. J. Ohanian, B. David, S. Taylor et al., "Piezoelectric morphing versus servo-actuated MAV control surfaces, part II: flight testing," in *51st AIAA Aerospace Sciences Meeting including the New Horizons Forum and Aerospace Exposition*, p. 0767, Dallas, TX, USA, 2013.

[10] K. B. Kochersberger, O. J. Ohanian III, T. Probst, and P. A. Gelhausen, "Design and flight test of the generic micro-aerial vehicle (GenMAV) utilizing piezoelectric conformal flight control actuation," *Journal of Intelligent Material Systems and Structures*, vol. 28, no. 19, pp. 2793–2809, 2017.

[11] D. Li, S. Guo, and J. Xiang, "Modeling and nonlinear aeroelastic analysis of a wing with morphing trailing edge," *Proceedings of the Institution of Mechanical Engineers, Part G: Journal of Aerospace Engineering*, vol. 227, no. 4, pp. 619–631, 2013.

[12] B. K. Stanford and P. S. Beran, "Analytical sensitivity analysis of an unsteady vortex-lattice method for flapping-wing optimization," *Journal of Aircraft*, vol. 47, no. 2, pp. 647–662, 2010.

[13] C. Xie, L. Wang, C. Yang, and Y. Liu, "Static aeroelastic analysis of very flexible wings based on non-planar vortex lattice method," *Chinese Journal of Aeronautics*, vol. 26, no. 3, pp. 514–521, 2013.

[14] R. L. Clark, M. R. Flemming, and C. R. Fuller, "Piezoelectric actuators for distributed vibration excitation of thin plates: a comparison between theory and experiment," *Journal of vibration and acoustics*, vol. 115, no. 3, pp. 332–339, 1993.

[15] J. Katz and A. Plotkin, *Low-Speed Aerodynamics, vol. 13*, Cambridge University Press, 2001.

[16] R. E. Melchers and A. T. Beck, *Structural Reliability Analysis and Prediction*, John Wiley & Sons, 2017.